

# Buckling analysis of laminated composite rectangular plates reinforced by SWCNTs using analytical and finite element methods<sup>†</sup>

A. Ghorbanpour Arani<sup>1,2,\*</sup>, Sh. Maghamikia<sup>1</sup>, M. Mohammadimehr<sup>1</sup> and A. Arefmanesh<sup>1</sup>

<sup>1</sup>Department of Mechanical Engineering, Faculty of Engineering, University of Kashan, Kashan, I. R. Iran

<sup>2</sup>Institute of Nanoscience & Nanotechnology, University of Kashan, Kashan, I.R. Iran

(Manuscript Received July 10, 2010; Revised December 1, 2010; Accepted December 5, 2010)

## Abstract

In this paper, the buckling analysis of laminated composite plates reinforced by single-walled carbon nanotubes (SWCNTs) is carried out using an analytical approach as well as the finite element method. The developed model is based on the classical laminated plate theory (CLPT) and the third-order shear deformation theory for moderately thick laminated plates. The critical buckling loads for the symmetrical layup are determined for different support edges. The Mori-Tanaka method is employed to calculate the effective elastic modulus of composites having aligned oriented straight nanotubes. The effect of the agglomeration of the randomly oriented straight nanotubes on the critical buckling load is also analyzed. The results of analytical solution are compared and verified with the FEM calculations. The critical buckling loads obtained by the finite element and the analytical methods for different layup and boundary conditions are in good agreement with each other. In this article, the effects of the carbon nanotubes (CNTs) orientation angle, the edge conditions, and the aspect ratio on the critical buckling load are also demonstrated using both the analytical and finite element methods.

**Keywords:** Buckling; FEM; Laminated composite; Rectangular plate; SWCNTs

## 1. Introduction

The buckling load of a laminated composite plate depends on a variety of parameters, such as, the properties of reinforcement, volume fraction and boundary conditions. Composites of carbon nanotubes (CNTs) dispersed in metallic or polymeric matrices have attracted a considerable attention in recent years. CNTs with their exceptional stiffness and strength have been regarded as an excellent candidate of reinforcements for advanced composites with high strength and low density. A number of experimental and theoretical studies have shown that CNTs have superior mechanical properties such as high stiffness to weight and strength to weight ratios, very high aspect ratio, and enormous electrical and thermal conductivities [1, 2]. Therefore, the presence of the nanotubes can improve the strength and stiffness of polymers as well as electrical and thermal conductivities to polymer based composite systems. Evidently, such composites are of paramount interest in aeronautic and astronautic technology, automobile and many other modern industries. Wang et al. [3] investigated the effective moduli of the CNT reinforced polymer

composite, with emphasis on the influence of CNT length and CNT-matrix interphase on the stiffening of the composite.

Tan et al. [4] investigated the effect of nonlinear interface debonding on the macroscopic behavior of the composite material with high particle volume fraction. They used the Mori-Tanaka method to study the constitutive behavior of the composite material.

The effect of van der Waals (vdW)-based interface cohesive law on carbon nanotube-reinforced composite materials was studied by Tan et al. [5]. Their results show that the increase of interface adhesion between CNTs and polymer matrix may significantly improve the composite behavior at the large strain.

Lu et al. [6] established the cohesive law for interfaces between MWCNTs and polymer that are not well bonded and are characterized by the vdW force. They concluded that the cohesive stress is dominated by the three carbon nanotube walls closest to the polymer.

Salehi-Khojin and Jalili [7] considered the buckling of boron nitride nanotube reinforced piezoelectric polymeric composites subjected to combined electro-thermo-mechanical loadings. Their results indicated that the piezoelectric matrix enhances the buckling resistance of composite significantly, and the supporting effect of elastic medium depends on the direction of applied voltage and thermal flow. Haque and Ra-

<sup>†</sup>This paper was recommended for publication in revised form by Editor Maenghyo Cho

\*Corresponding author. Tel.: +98 913 162 6594, Fax.: +98 361 555 9930

E-mail address: aghorban@kashanu.ac.ir

© KSME & Springer 2011

masetty [8] developed an analytical model to study stress transfer in SWCNT reinforced polymer matrix composites and their model can be used to predict axial stress and interfacial shear stress along the CNT embedded in matrix materials. Moreover, they considered the effects of CNT aspect ratio, CNT volume fraction and matrix modulus on axial stress and interfacial shear stress and also compared the results of this analytical model with finite element analysis.

Nanomechanical properties of coiled CNT reinforced epoxy composites were investigated by Li et al. [9]. Their results show that the hardness, elastic modulus and tensile strength of the coiled CNT/epoxy composite increase with increasing the weight percentage of the CCNTs.

Ke et al. [10] investigated the nonlinear free vibration of functionally graded nanocomposite beams reinforced by SWCNTs based on Timoshenko beam theory and von Karman geometric nonlinearity. Sofiyev [11] investigated the torsional buckling problem of cross-ply laminated cylindrical thin shells, made of orthotropic composite materials, subjected to loads varying as a power function of time, by using the Ritz type variational method. He obtained the modified Donnell type dynamic stability and compatibility equations and reduced these equations to a time dependent differential equation with variable coefficients by using Galerkin's method. Ozben [12] calculated the critical buckling load value of fiber reinforced composite plate by analytical and finite element methods. He obtained the composite deformation behavior and critical buckling values according to  $L_x/L_y$  ratio in plate dimension. Shen and Zhang [13] studied thermal post-buckling behavior of functionally graded carbon nanotube-reinforced composite plates subjected to in-plane temperature variation based on a micromechanical model and multi-scale approach. The results presented in this article indicate that the thermal post-buckling behaviors of carbon nanotube-reinforced composite (CNTRC) plates are significantly influenced by the thermal load ratio, the transverse shear deformation, the plate aspect ratio as well as the nanotube volume fraction.

Motivated by these considerations, we aim to study the buckling behavior of composite plate reinforced by SWCNTs under uniaxial compressive load by using finite element and analytical methods. The material properties of SWCNTs are obtained using the Mori-Tanaka method. The effect of agglomeration of CNTs on the critical buckling load is investigated using analytical micromechanics methods. It will be shown agglomeration of CNTs have significant influence on the buckling load and properties of CNTRC.

## 2. Effective modulus of the composite

In this section, the effective modulus of the composite plate reinforced by CNTs is developed. Different methods are available to estimate the overall properties of a composite. The Mori-Tanaka [14] method is employed in this section due to its simplicity and accuracy even at high volume fractions of

the inclusions. Initially, the nanotubes are assumed to be aligned and straight with a uniform dispersion in the polymer. The matrix is assumed to be elastic and isotropic, with the Young's modulus  $E_m$  and the Poisson's ratio  $\nu_m$ .

The constitutive relations for a layer of the composite with the principal axes parallel to the  $x$ -,  $y$ -, and  $z$ - directions are [15]:

$$\begin{bmatrix} \sigma_{xx} \\ \sigma_{yy} \\ \tau_{yz} \\ \tau_{xz} \\ \tau_{xy} \end{bmatrix} = \begin{bmatrix} Q_{11} & Q_{12} & 0 & 0 & 0 \\ Q_{12} & Q_{22} & 0 & 0 & 0 \\ 0 & 0 & Q_{44} & 0 & 0 \\ 0 & 0 & 0 & Q_{55} & 0 \\ 0 & 0 & 0 & 0 & Q_{66} \end{bmatrix} \begin{bmatrix} \varepsilon_{xx} \\ \varepsilon_{yy} \\ \gamma_{yz} \\ \gamma_{xz} \\ \gamma_{xy} \end{bmatrix}, \quad (1)$$

where  $\sigma_{ij}$ ,  $\varepsilon_{ij}$  and  $Q_{ij}$  are the stress components, the strain components and the stiffness coefficients, respectively. According to the Mori-Tanaka method the stiffness coefficients are given by [16]:

$$\begin{aligned} Q_{11} &= \frac{E_m^2 c_m (1+c_r - c_m \nu_m) + 2c_m c_r (k_r n_r - l_r^2)(1+\nu_m)^2 (1-2\nu_m)}{(1+\nu_m)\{2c_m k_r (1-\nu_m - 2\nu_m^2) + E_m (1+c_r - 2\nu_m)\}} \\ &\quad + \frac{E_m [2c_m^2 k_r (1-\nu_m) c_r n_r (1-2\nu_m + c_r) - 4c_m l_r \nu_m]}{2c_m k_r (1-\nu_m - 2\nu_m^2) + E_m (1+c_r - 2\nu_m)}, \\ Q_{22} &= \frac{E_m \{E_m c_m + 2k_r (1+\nu_m)[1+c_r (1-2\nu_m)]\}}{2(1+\nu_m)[E_m (1+c_r - 2\nu_m) + 2c_m k_r (1-\nu_m - 2\nu_m^2)]} \\ &\quad + \frac{E_m [E_m c_m + 2m_r (3+c_r - 4\nu_m)(1+\nu_m)]}{2(1+\nu_m)\{E_m [c_m + 4c_r (1-\nu_m)] + 2m_r c_m (3+c_r - 4\nu_m^2)\}}, \\ Q_{12} &= \frac{E_m \{c_m \nu_m [E_m + 2k_r (1+\nu_m)] + 2c_r l_r (1-\nu_m^2)\}}{(1+\nu_m)[2c_m k_r (1-\nu_m - 2\nu_m^2) + E_m (1+c_r - 2\nu_m)]}, \\ Q_{44} &= \frac{E_m [E_m c_m + 2m_r (3+c_r - 4\nu_m)(1+\nu_m)]}{2(1+\nu_m)\{E_m [c_m + 4c_r (1-\nu_m)] + 2m_r c_m (3+c_r - 4\nu_m^2)\}}, \\ Q_{55} = Q_{66} &= \frac{E_m [E_m c_m + 2(1+c_r) p_r (1+\nu_m)]}{2(1+\nu_m)[E_m (1+c_r) + 2c_m p_r (1+\nu_m)]}, \end{aligned} \quad (2)$$

where  $c_m$  and  $c_r$  are the volume fractions of the matrix and the CNTs respectively. In the above equations,  $k_r$ ,  $l_r$ ,  $m_r$ ,  $n_r$  and  $p_r$  are the Hill's elastic modulus for the CNTs [16].

The reduced transformed stiffness coefficient matrix is [15]:

$$[\bar{Q}_{ij}] = [T][Q_{ij}][T]^{-1}, \quad (3)$$

where  $[T]$  is the transformed matrix which is given by [15]:

$$[T] = \begin{bmatrix} \cos^2 \theta & \sin^2 \theta & 0 & 0 & 0 & -\sin 2\theta \\ \sin^2 \theta & \cos^2 \theta & 0 & 0 & 0 & \sin 2\theta \\ 0 & 0 & 1 & 0 & 0 & 0 \\ 0 & 0 & 0 & \cos \theta & \sin \theta & 0 \\ 0 & 0 & 0 & -\sin \theta & \cos \theta & 0 \\ \sin \theta \cos \theta & 0 & 0 & 0 & 0 & \cos^2 \theta - \sin^2 \theta \end{bmatrix}. \quad (4)$$

### 3. Analytical solution

The CLPT is used to obtain the analytical solution because it is simple to use for moderately thick cross ply laminated plates. The length, the width, and the thickness of the plate are denoted by  $a$ ,  $b$  and  $h$ , respectively. The edges of the plate can be either simply and clamped supported or free.

#### 3.1. Total potential energy

The total potential energy of the plate, due to the internal strain and the surface traction, is given by [17]:

$$\Pi = \int_V \{\varepsilon\}^T \{\sigma\} dV + \int_A \{\varphi\}^T \{t\} dA \tag{5}$$

The first term in the right hand-side of Eq. (5) is the strain energy which  $V$  denoting the volume of the plate. The second term is the energy originated by surface traction which  $A$  being the portions of plate surface over which tractions are prescribed.  $\{\varphi\}$  is displacement vector and  $\{t\}$  is the surface traction.

The constitutive relating the stress and the strain can be written as

$$\{\sigma\} = [C] \{\varepsilon\}, \tag{6}$$

where  $[C]$  is the elastic tensor whose components are given by [15]:

$$C_{11} = \sum_{k=1}^n [\bar{Q}_{11}]_k, C_{22} = \sum_{k=1}^n [\bar{Q}_{22}]_k, C_{12} = \sum_{k=1}^n [\bar{Q}_{12}]_k, \\ C_{66} = \sum_{k=1}^n [\bar{Q}_{66}]_k, C_{16} = \sum_{k=1}^n [\bar{Q}_{16}]_k, C_{26} = \sum_{k=1}^n [\bar{Q}_{26}]_k, \tag{7}$$

where  $k$  denotes the layer number. According to Eqs. (6) and (7), the strain energy can be written as:

$$U = \frac{1}{2} \int_R [\varepsilon]^T [Q] \{\varepsilon\} dV = \\ \frac{1}{2} \int_R \begin{bmatrix} \varepsilon_x & \varepsilon_y & \varepsilon_{xy} \end{bmatrix} \begin{bmatrix} C_{11} & C_{12} & C_{13} \\ C_{21} & C_{22} & C_{23} \\ C_{31} & C_{32} & C_{33} \end{bmatrix} \begin{bmatrix} \varepsilon_x \\ \varepsilon_y \\ \varepsilon_{xy} \end{bmatrix} dV. \tag{8}$$

The relations between the strain and the displacement in the CLPT are given by [17]:

$$\varepsilon_x = \frac{\partial u_0}{\partial x} - z \frac{\partial^2 w}{\partial x^2}, \\ \varepsilon_y = \frac{\partial v_0}{\partial y} - z \frac{\partial^2 w}{\partial y^2}, \\ \varepsilon_{xy} = \frac{\partial u_0}{\partial x} + \frac{\partial v_0}{\partial y} - 2z \frac{\partial^2 w}{\partial x \partial y}, \tag{9}$$

where  $u_0$  and  $v_0$  are the displacements of the mid-plane in  $x$ - and  $y$ - directions, respectively, which are assumed to

be zero because there is no coupling between the in-plane and the out-of-plane displacements.  $w(x, y)$  denotes the displacement in  $z$ - direction, i.e. the lateral deflection of the composite plate. Substituting Eq. (9) into Eq. (8) yields:

$$U = \frac{1}{2} \int_0^a \int_0^b \int_{-\frac{h}{2}}^{\frac{h}{2}} \left\{ \begin{aligned} & z^2 \sum_{k=1}^n [\bar{Q}_{11}]_k \left( \frac{\partial^2 w}{\partial x^2} \right)^2 + 2z^2 \sum_{k=1}^n [\bar{Q}_{12}]_k \left( \frac{\partial^2 w}{\partial x^2} \right) \left( \frac{\partial^2 w}{\partial y^2} \right) + \\ & 2z^2 \sum_{k=1}^n [\bar{Q}_{26}]_k \left( \frac{\partial^2 w}{\partial y^2} \right) \left( \frac{2\partial^2 w}{\partial x \partial y} \right) + \\ & 2z^2 \sum_{k=1}^n [\bar{Q}_{16}]_k \left( \frac{\partial^2 w}{\partial x^2} \right) \left( \frac{2\partial^2 w}{\partial x \partial y} \right) + \\ & z^2 \sum_{k=1}^n [\bar{Q}_{22}]_k \left( \frac{\partial^2 w}{\partial y^2} \right)^2 + z^2 \sum_{k=1}^n [\bar{Q}_{66}]_k \left( \frac{2\partial^2 w}{\partial x \partial y} \right)^2 \end{aligned} \right\} dx dy dz. \tag{10}$$

The surface traction is given by [17]:

$$W = \int_A \{\varphi\}^T \{t\} dA = \int_0^a \int_0^b \left\{ \begin{aligned} & N_x \left[ \frac{\partial u_0}{\partial x} + \frac{1}{2} \left( \frac{\partial w}{\partial x} \right)^2 \right] + N_y \left[ \frac{\partial v_0}{\partial y} + \frac{1}{2} \left( \frac{\partial w}{\partial y} \right)^2 \right] \\ & + N_{xy} \left[ \left( \frac{\partial u_0}{\partial y} + \frac{\partial v_0}{\partial x} \right) + \left( \frac{\partial w}{\partial x} \right) \left( \frac{\partial w}{\partial y} \right) \right] \end{aligned} \right\} dx dy, \tag{11}$$

where  $N_x$  and  $N_y$  are the resultant forces in the  $x$ - and  $y$ - directions, respectively and  $N_{xy}$  denotes the shear force.  $N_x$  and  $N_{xy}$  are assumed to be zero. Substituting Eqs. (10) and (11) in Eq. (5) yields the following simplified expression for the total potential energy under axial compression [15]:

$$\Pi = \frac{1}{2} \int_0^a \int_0^b \left\{ \begin{aligned} & D_{11} \left( \frac{\partial^2 w}{\partial x^2} \right)^2 + 2D_{12} \left( \frac{\partial^2 w}{\partial x^2} \right) \left( \frac{\partial^2 w}{\partial y^2} \right) + D_{22} \left( \frac{\partial^2 w}{\partial y^2} \right)^2 \\ & + D_{66} \left( \frac{\partial^2 w}{\partial x \partial y} \right)^2 + N_x \left( \frac{\partial w}{\partial x} \right)^2 \end{aligned} \right\} dx dy, \tag{12}$$

where  $D_{ij}$  is the bending stiffness matrix whose elements are given by [15]:

$$D_{ij} = \sum_{k=1}^n \int_{z_k}^{z_{k-1}} \bar{Q}_{ij}^k z^2 dz. \tag{13}$$

It is noted that  $D_{16}$  and  $D_{26}$  in Eq. (12) are eliminated in orthotropic plates [15].

$N_x$  in Eq. (13), is the axial compressive load in the  $x$ - direction which is a function of the buckling parameter ( $\lambda$ ) and the edge load. It is given by [17]:

$$N_x = \lambda N_{x0}. \tag{14a}$$

The edge load is defined as:

$$N_{x0} = \frac{n(10h)^3}{3a^2}, \tag{14b}$$

where  $n$  is the uniaxial tension modulus in the fiber direction.

$h$  and  $a$  are the length of side and thickness of the plate which are equal to  $1.5\text{mm}$  and  $25\text{mm}$ , respectively.

According to the Levy solution [17], it is important to find suitable function for the lateral deflection. It is assumed that the lateral deflection can be written as the following separate function of  $x$  and  $y$  variables:

$$w(x, y) = f(x)g(y). \tag{15}$$

For the simply-supported boundary conditions at the four edges ( $s-s-s-s$ ), the lateral deflection is written as [17]:

$$w(x, y) = \sum_{n=1}^{\infty} \sum_{m=1}^{\infty} A_{mn} \sin \frac{n\pi x}{a} \sin \frac{m\pi y}{b}, \tag{16}$$

where  $A_{mn}$  is the deflection amplitude, and  $n$  and  $m$  are the number of half sine waves in the  $x$ - and  $y$ - directions, respectively.

Substituting the solution  $w(x, y)$  from Eq. (16) into Eq. (12) results in:

$$\Pi = \frac{1}{2} \int_0^a \int_0^b \left\{ \begin{aligned} &D_{11} \left( \frac{n\pi}{a} \right)^4 \sum_{n=1}^{\infty} \sum_{m=1}^{\infty} A_{mn}^2 \left( \sin \frac{n\pi x}{a} \right)^2 \left( \sin \frac{m\pi y}{b} \right)^2 \\ &+ D_{22} \left( \frac{m\pi}{b} \right)^4 \sum_{n=1}^{\infty} \sum_{m=1}^{\infty} A_{mn}^2 \left( \sin \frac{n\pi x}{a} \right)^2 \left( \sin \frac{m\pi y}{b} \right)^2 \\ &+ 2D_{12} \left( \frac{n\pi}{a} \right)^2 \left( \frac{m\pi}{b} \right)^2 \sum_{n=1}^{\infty} \sum_{m=1}^{\infty} A_{mn}^2 \left( \sin \frac{n\pi x}{a} \right)^2 \left( \sin \frac{m\pi y}{b} \right)^2 \\ &+ 4D_{66} \left( \frac{n\pi}{a} \right)^2 \left( \frac{m\pi}{b} \right)^2 \sum_{n=1}^{\infty} \sum_{m=1}^{\infty} A_{mn}^2 \left( \cos \frac{n\pi x}{a} \right)^2 \left( \cos \frac{m\pi y}{b} \right)^2 \\ &- N_x \left( \frac{n\pi}{a} \right)^2 \sum_{n=1}^{\infty} \sum_{m=1}^{\infty} A_{mn}^2 \left( \cos \frac{n\pi x}{a} \right)^2 \left( \sin \frac{m\pi y}{b} \right)^2 \end{aligned} \right\} dx dy. \tag{17}$$

For the plate to be in equilibrium, the total energy should be stationary:

$$\frac{\partial \Pi}{\partial A_{mn}} = 0. \tag{18}$$

Hence, solving Eq. (18) yield the following buckling load:

$$N_{x,cr} = \lambda_{cr} N_{x0} = \frac{\pi^2}{b^2} \left[ D_{11} \frac{b^2}{a^2} + D_{22} \frac{a^2}{b^2} + 2(D_{11} + 2D_{66}) \right]. \tag{19}$$

The critical axial buckling loads for different boundary conditions, which are obtained by minimizing the total potential energy of the plate, are presented in Table 1.

#### 4. The effect of agglomeration

Due to small diameter and small elastic modulus in the radial direction and high aspect ratio, CNTs have low bending stiffness and can easily agglomerate in the polymer matrix. In fact, there are some local regions in the composite which have

higher concentration of CNTs than the average volume fraction. These regions, which have spherical shapes, are called “inclusion” [16]. In this section, material properties of CNTRC plates with random dispersion of CNTs are developed and the effect of agglomeration of CNTs on the effective material properties is studied. The Random dispersion of CNTs renders the composite isotropic with two effective elastic modulus, namely, the effective bulk modulus and effective shear modulus [16]:

$$\begin{aligned} k &= k_{out} \left[ 1 + \frac{\xi \left( \frac{k_{in}}{k_{out}} - 1 \right)}{1 + \alpha(1 - \xi) \left( \frac{k_{in}}{k_{out}} - 1 \right)} \right], \\ G &= G_{out} \left[ 1 + \frac{\xi \left( \frac{G_{in}}{G_{out}} - 1 \right)}{1 + \beta(1 - \xi) \left( \frac{G_{in}}{G_{out}} - 1 \right)} \right]. \end{aligned} \tag{20}$$

The effective bulk modulus  $k_{in}$  and  $k_{out}$ , and the effective shear modulus  $G_{in}$  and  $G_{out}$  in the inclusions and out of the inclusions are given by [16]:

$$\begin{aligned} k_{in} &= k_m + \frac{(\delta_r - 3k_m \alpha_r) c_r \zeta}{3(\xi - c_r \zeta + c_r \zeta \alpha_r)}, \\ k_{out} &= k_m + \frac{c_r (\delta_r - 3k_m \alpha_r) (1 - \zeta)}{3[1 - \xi - c_r (1 - \zeta) + c_r (1 - \zeta) \alpha_r]}, \\ G_{in} &= G_m + \frac{c_r \zeta (\eta_r - 2G_m \beta_r)}{2(\xi - c_r \zeta + c_r \zeta \beta_r)}, \\ G_{out} &= G_m + \frac{c_r (1 - \zeta) (\eta_r - 2G_m \beta_r)}{2[1 - \zeta - c_r (1 - \zeta) + c_r (1 - \zeta) \beta_r]}, \end{aligned} \tag{21}$$

where  $\zeta$  denotes the volume ratio of CNTs that are dispersed in inclusion and the total volume of the nanotubes,  $\zeta$  denotes the volume fraction of inclusions with respect to the total volume of the representative volume element and  $\alpha$ ,  $\beta$ ,  $\delta_r$ ,  $\alpha_r$ ,  $\beta_r$  and  $\eta_r$  which are functions of the bulk modulus matrix and shear modulus ( $k_m$ ,  $G_m$ ) are presented in the Ref. [16].

#### 5. The FEM solution

The critical buckling load is derived using the Bodyanski method [18]. For a moderately thick plate using a higher shear deformation theory leads to better results. In this work, the third-order shear deformation theory developed by Reddy is used so that the strain equations don't need a shear correction factor which is required in a first-order shear deformation theory. The displacement field can be expressed as [19]:

$$\begin{aligned}
 u(x, y, z) &= u_0(x, y) + z\phi_x(x, y) - \frac{4}{3h^2}z^3\left(\phi_x(x, y) + \frac{\partial w_0(x, y)}{\partial x}\right), \\
 v(x, y, z) &= v_0(x, y) + z\phi_y(x, y) - \frac{4}{3h^2}z^3\left(\phi_y(x, y) + \frac{\partial w_0(x, y)}{\partial y}\right), \\
 w(x, y, z) &= w_0(x, y),
 \end{aligned}
 \tag{22}$$

where  $u_0(x, y)$  and  $v_0(x, y)$  are the displacements of the mid-plane in  $x$ - and  $y$ - directions, respectively, and  $w_0(x, y)$  denotes displacement in  $z$ - direction.  $\phi_x(x, y)$  and  $\phi_y(x, y)$  are the rotations of the normal to the mid-plane about  $x$ - and  $y$ - directions, respectively. The Von Karman strains for the case of in plane strain are composed of linear,  $\{\epsilon_0\}$  and nonlinear,  $\{\epsilon_1\}$  strains [20]:

$$\{\epsilon\} = \{\epsilon_0\} + \{\epsilon_1\} = \begin{bmatrix} \epsilon_x \\ \epsilon_y \\ \gamma_{zy} \\ \gamma_{xz} \\ \gamma_{xy} \end{bmatrix} = \begin{bmatrix} u_x \\ u_y \\ w_y + u_z \\ u_z + w_x \\ u_y + v_x \end{bmatrix} + \begin{bmatrix} \frac{1}{2}(w_x)^2 \\ \frac{1}{2}(w_y)^2 \\ 0 \\ 0 \\ w_x w_y \end{bmatrix}. \tag{23}$$

It can be expressed in the following form

$$\{\epsilon\} = ([d^0] + z[d^1] + z^2[d^2] + z^3[d^3])\{\varphi\}, \tag{24}$$

where  $\{\varphi\}^T = \langle u_0 \ v_0 \ w_0 \ \phi_x \ \phi_y \rangle$ , and the matrix  $[d^i]$  (derivation matrix) are given in Appendix A .

Using Eq. (5), the variation of the total potential energy of the plate, due to the internal strain and the surface traction, can be expressed as:

$$\delta\Pi = \int_V \delta(\{\epsilon\}^T)\{\sigma\}dV + \int_A \delta(\{\varphi\}^T)\{t\}dA. \tag{25}$$

Using the shape function matrix  $[N]$ , the displacement is interpolated by [20]:

$$\{\varphi\} = [N]\{\Phi^{(e)}\}, \tag{26}$$

where  $\{\Phi^{(e)}\}$  is the vector of unknown nodal values and the matrix  $[B^i]$  are given by [20]:

$$[B^i] = [d^i][N]. \tag{27}$$

The shape function matrix ( $[N]$ ) and the matrix  $[B^i]$  are given in Appendix A. Substituting Eqs. (25), (27) and (28) into Eq. (26) yields:

$$\left( \int_V ([B^0]^T + z[B^1]^T + z^2[B^2]^T + z^3[B^3]^T) \bar{Q} ([B^0] + z[B^1] + z^2[B^2] + z^3[B^3]) dV \right) \{\Phi^{(e)}\} - \int_A [N]^T \{t\} dA \{\Phi^{(e)}\} = 0. \tag{28}$$

The stiffness matrix and the load vector for each element are given by

$$\begin{aligned}
 [K^{(e)}] &= \int_V ([B^0]^T + z[B^1]^T + z^2[B^2]^T \\
 &\quad + z^3[B^3]^T) \bar{Q} ([B^0] + z[B^1] \\
 &\quad + z^2[B^2] + z^3[B^3]) dV,
 \end{aligned}
 \tag{29}$$

$$\{W^{(e)}\} = \int_A [N]^T \{t\} dA. \tag{30}$$

The stress with respect to the strain is plotted, and according to bodyanski method [18] the region where the slope of the curve increases severely denotes the critical buckling load. Tables 2 and 4 show a comparison between the results of the FEM and the analytical solution.

### 6. Results and discussion

In this work, the buckling of a composite plate reinforced by CNTs is investigated by the finite element and the analytical method. The results are presented for four different kinds of boundary conditions. The composite plate is composed of polystyrene as the matrix with the Young’s modulus and the Poisson’s ratio of  $E_m = 1.9\text{Gpa}$ , and  $\nu_m = 0.3$ , respectively. The CNTs are modeled as long, transversely isotropic fibers based on the analytical result of Popov et al. [21]. The material properties of SWCNTs are:

$$\begin{aligned}
 k_r &= 30\text{Gpa}, l_r = 10\text{Gpa}, m_r = 1\text{Gpa}, \\
 n_r &= 450\text{Gpa}, p_r = 1\text{Gpa}.
 \end{aligned}
 \tag{31}$$

The results of the finite element and the analytical methods are quite close to each other. However, the analytical results show a lower critical buckling load because of eliminating the shear strain in the classical plate theory. Tables 2 and 4 show a comparison between the results of the finite element and the analytical solutions. In these tables, the longitudinal, and the transversal mode shapes are assumed to be equal to one ( $n, m = 1$ ), and CNTs are arranged in  $45^\circ$  direction with respect to load direction and with the aspect ratio of unit. The results are given for four different boundary conditions, and three volume fractions of CNTs. It is clear from the results that the critical axial buckling load increases with increasing the volume fraction. Therefore, the highest critical axial buckling load occurs at  $c_r = 0.1$  for each boundary condition. The effects of CNTs orientation and the laminated layup for different boundary conditions are discussed next.

Fig. 1 shows the effect of the aspect ratio on the critical buckling load for different longitudinal mode shapes. There are three plots for three boundary conditions in this figure. For each boundary condition, increasing the aspect ratio causes the buckling to occur in a higher mode shape. By changing one of the edges parallel to load direction to the clamped support, at a

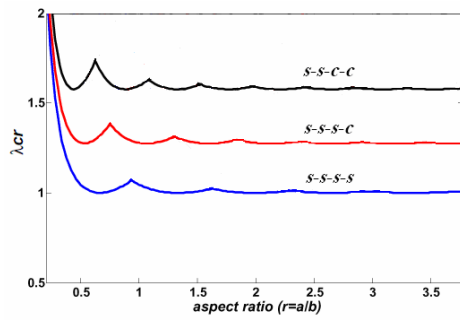


Fig. 1. Effect of aspect ratio on the critical buckling load for different boundary condition.

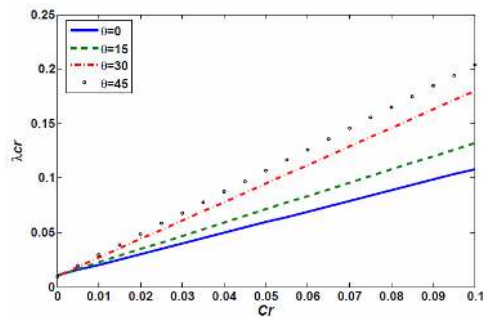


Fig. 2. Effect of the orientation angle and CNTs volume fraction on the critical buckling load for one layer composite plate.

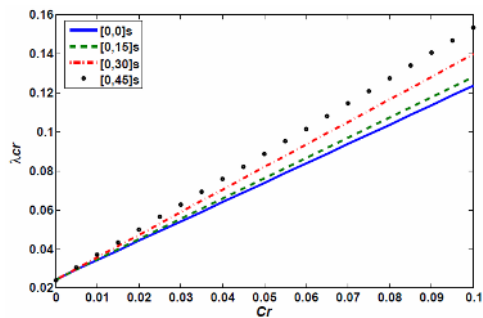
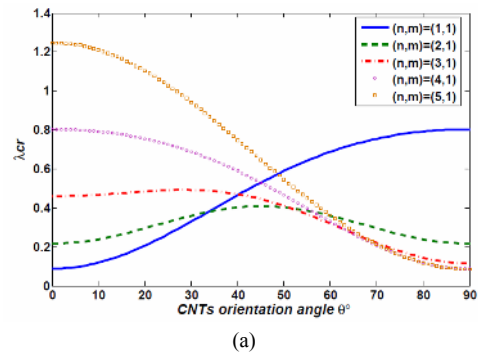


Fig. 3. Effect of laminated layup and CNTs volume fraction on the critical buckling load for symmetric layup composite plate.

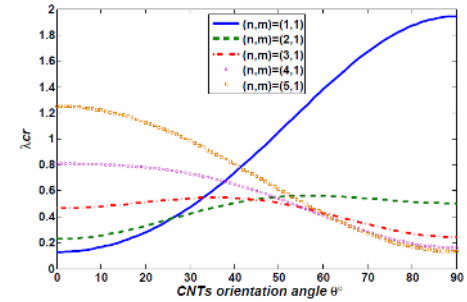
constant aspect ratio, the critical buckling load increases with increasing the longitudinal mode shape.

Fig. 2 shows the effect of the orientation angle and the volume fraction of the CNTs on the critical buckling load for one layer composite plate. It is seen that the highest critical load occurs when the CNTs are arranged in 45° direction. Fig. 3 depicts the effect of the laminated layup and the volume fraction of the CNTs on the critical buckling load for symmetric layup composite plate. This layup ([0,45]<sub>s</sub>) causes to the most stable state.

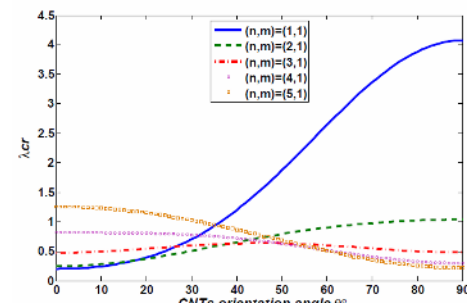
Figs. 4 and 5 show the effects of the CNTs orientation angle and the mode shape on the critical buckling load for different aspect ratios and boundary conditions. The variation of the buckling load with respect to the orientation angle is different for different mode shapes. Fig. 4 is for the aspect ratio of



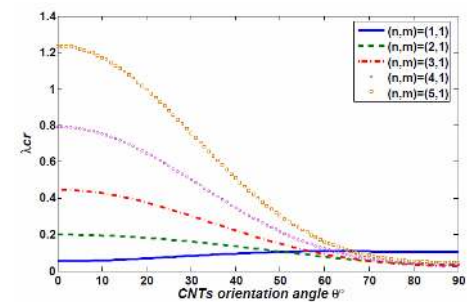
(a)



(b)



(c)



(d)

Fig. 4. Effect of the nanotubes orientation on the critical buckling load for different mode shape, at aspect ratio  $a/b=2$  and different kinds of edge supports: (a)  $s-s-s-s$ , (b)  $s-s-c-s$ , (c)  $s-s-c-c$ , and (d)  $s-s-c-f$ .

$a/b=2$ . For example, in Fig. 4(a) for ( $s-s-s-s$ ) supported, for the first mode shape, the stability of the plate increases with increasing the orientation angle from 0° to 90°; while, for the other mode shape, the stability of the plate increases with decreasing the orientation angle from 0° to 90°. For this case, whenever the CNTs are arranged in 33° direction, the buckling is in the first mode, between 33° to

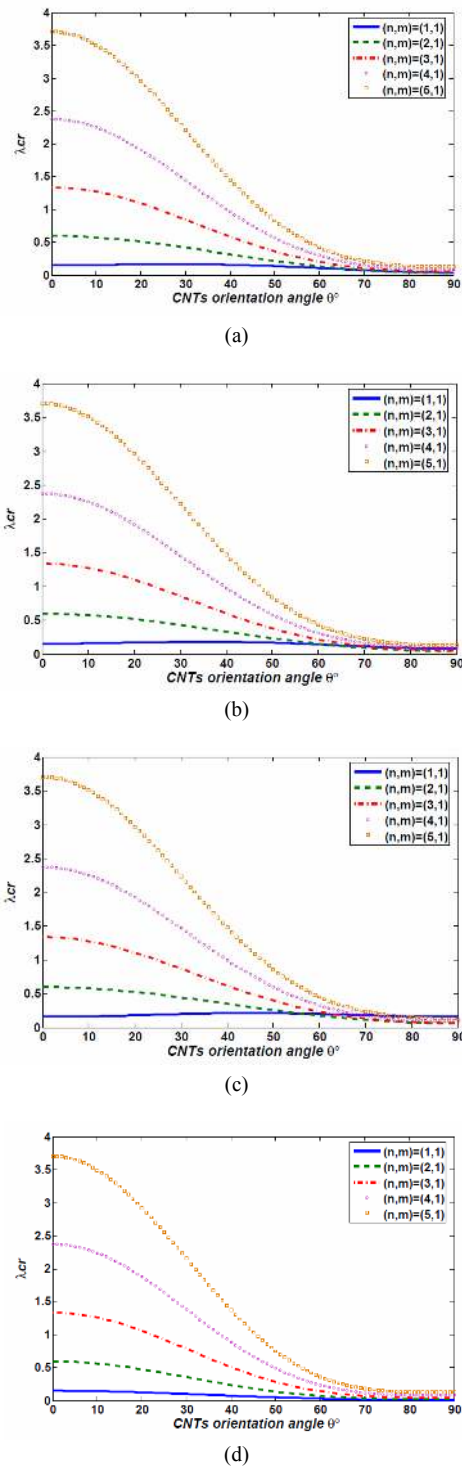


Fig. 5. Effect of the nanotubes orientation on the critical buckling load for different mode shapes, at aspect ratio  $a/b=2/3$  and different kinds of edge supports: (a) s-s-s-s, (b) s-s-c-s, (c) s-s-c-c, and (d) s-s-c-f.

54° it is in the second mode, and as the orientation angles increases the buckling occurs in further mode shapes. These results are shown in this Fig. for four boundary conditions. For (s-s-s-s) supported and CNTs orientation angle 45°, the buck-

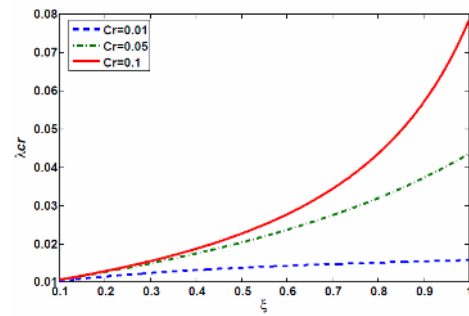


Fig. 6. Effect of the CNTs agglomeration on the critical buckling for three different volume fractions of CNTs with  $\zeta = 1$ .

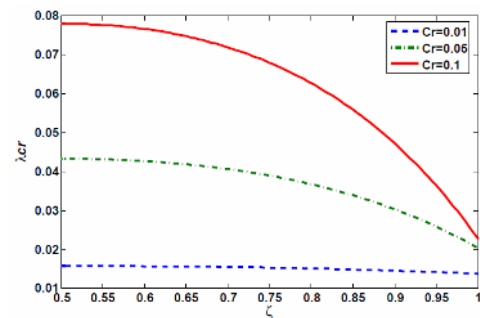


Fig. 7. Effect of the CNTs agglomeration on the critical buckling for three different volume fractions of CNTs with  $\xi = 0.5$ .

ling occurs in the second mode. When one of the edges change from simply supported to the clamped support (s-s-s-c) results in buckling loads occur at lower angles. In case one of the edges be free (s-s-c-f), the critical load decreases and the buckling occur in the first mode for the angles below 60°. In Fig. 5, the aspect ratio is changed to  $a/b=2/3$ , while the volume of the plate and the volume fraction of the CNTs are kept constant for each aspect ratio. The buckling load, the mode shape, and the corresponding angles for other aspect ratios, and boundary condition are presented in Table 3.

Figs. 6 and 7 show the effect of the CNTs agglomeration on the buckling load of the plate. Increasing  $\xi$  in Fig. 6 results in a uniform distribution of inclusions. Hence, the nanotubes disperse more uniformly and the critical buckling load increases. The results in this figure are presented for three different volume fractions of CNTs. Increasing  $\zeta$  in Fig. 7 leads to non-uniform dispersion of the CNTs; hence, the critical buckling load decreases by increasing the  $\zeta$ . Similar to Fig. 6, the results in this figure are presented for three different volume fractions. The buckling load increases drastically for higher volume fractions.

Fig. 8 shows the effect of the thickness-to-width ratio on the critical buckling load for different boundary conditions. The critical buckling load increases exponentially for all boundary conditions, and the slope of the curves increases severely in high volume fractions as the thickness of plate increases.

Table 2 compares the results of the analytical method with

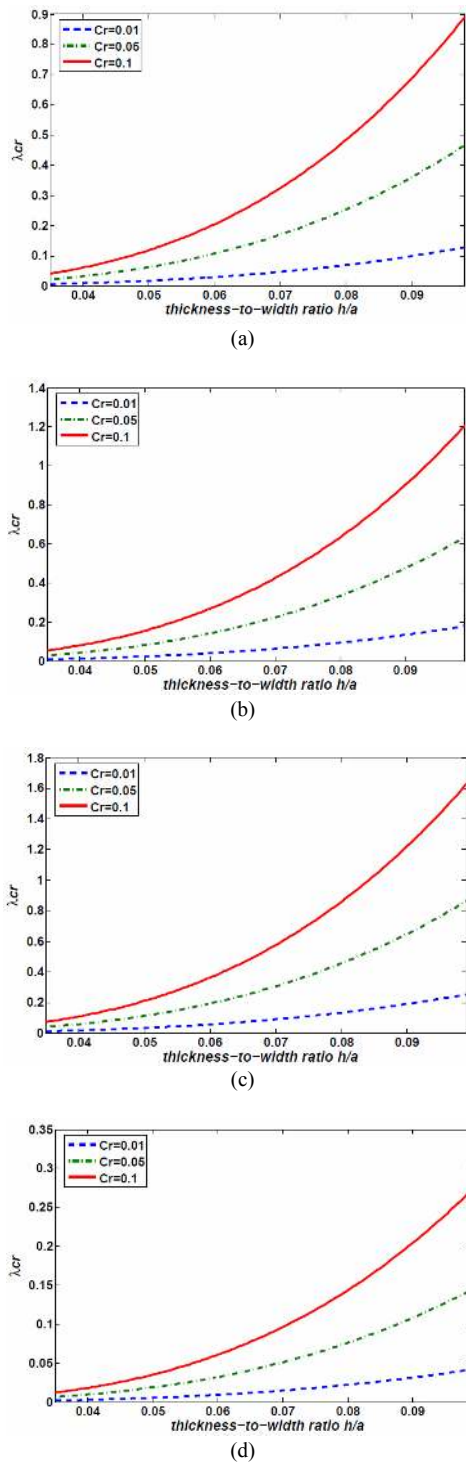


Fig. 8. The effect of thickness to width on the critical buckling load of CNTRC composite plate with different boundary condition: (a) s-s-s-s, (b) s-s-c-s, (c) s-s-c-c, and (d) s-s-c-f.

those of the FEM for different boundary conditions and different volume fractions of CNTs. As stated before, the CLPT is used in the analytical method, and the third order Reddy plate theory is employed for the FEM. So, even though the results of the two methods are in good agreement, the finite element

results are lower than the results of analytical method due to eliminating the shear strains in the analytical method.

Table 3 shows the effect of the CNTs orientation angle on the buckling load for different mode shapes, aspect ratios, and boundary conditions. Even though the ratio of width to length is varied, the thickness and the total area of the plate and the CNTs volume fraction remain constant for each aspect ratio and boundary condition. Therefore, it is possible to compare the different kinds of boundary conditions and choose the optimized aspect ratio and CNTs orientation angle to achieve the highest critical buckling load. For each aspect ratio, the mode shape and the corresponding angle that make the plate unstable are determined for four different boundary conditions. Moreover, the special mode shape, and the CNTs orientation angle corresponding to the highest critical buckling load is obtained for each aspect ratio and boundary condition. For example, for s-s-s-s edges and the width-to-length ratio of  $a/b=2$ , whenever the CNTs orientation angle is less than  $34^\circ$ , the buckling occurs in the first mode; between  $34^\circ$  to  $53^\circ$  it occurs in the second mode and in this manner the buckling load increases as the CNTs orientation angle increases. For other angles, the corresponding mode shapes are presented in Table 3. The highest critical buckling load in this case occurs for the  $45^\circ$  angle, and in the second mode shape. According to this table, as the aspect ratio decreases from 2 to  $1/2$ , the highest critical buckling load decreases. Moreover, there is no change in the mode shape for different CNTs orientation angles. Changing the longitudinal edges from simple to clamped increases the stability of plate, and changing it to free boundary condition, results in less buckling loads. Therefore, for all kinds of boundary conditions except the (s-s-c-f) supported case, the highest critical buckling occurs at  $a/b=2$ . For the case of (s-s-s-s) boundary condition, the critical load which is in the second mode and  $45^\circ$  CNTs orientation angle is  $N_{cro} = 834N$ . For the case of (s-s-s-c) supported, the critical load which is also in the second mode and  $48^\circ$  CNTs orientation angle is  $N_{cro} = 1120.2N$ . For the (s-s-c-c) supported case, the critical load which is in the third mode and  $45^\circ$  CNTs orientation angle is  $N_{cro} = 1304.4N$ . Contrary to mentioned boundary conditions, for the case of s-s-c-f, the highest critical buckling load which is in the first mode and  $0^\circ$  CNTs orientation angle occurs at  $a/b=1/2$  is  $N_{cro} = 404.74N$ .

Table 4 shows the effect of CNTs agglomeration on the critical buckling load. The CNTs are assumed to be dispersed randomly so that the composite is isotropic and only two material constants are required for predicting its behavior. The volume fraction of the CNTs and the orientation angle are considered to be constant. The first three columns of the table are for the inclusion volumes of unit ( $\zeta = 1$ ), and the critical buckling load is given for three kinds of inclusion dispersions. For the remaining three columns, inclusions are dispersed uniformly and the critical loads are determined for three different CNTs volume ratios.



Table 1. The critical axial buckling load for different boundary conditions [15].

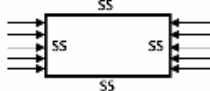
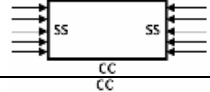
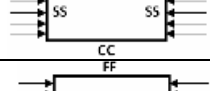
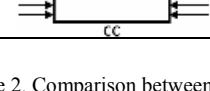
Different boundary conditions	The critical axial buckling load	Displacement function
	$\pi^2 \left[ D_{11} \frac{n^2}{a^2} + D_{22} \frac{a^2}{n^2 b^4} + 2(D_{11} + 2D_{66}) \right]$	$w(x, y) = \sum_{n=1}^{\infty} \sum_{m=1}^{\infty} A_{mn} \sin \frac{n\pi x}{a} \sin \frac{m\pi y}{b}$
	$\pi^2 \left[ D_{11} \frac{n^2}{a^2} + 2.441D_{22} \frac{a^2}{n^2 b^4} + 2.33(D_{11} + 2D_{66}) \right]$	$w(x, y) = \sum_{n=1}^{\infty} A_n [b^3 y - 3by^3 + 2y^4] \sin \frac{n\pi x}{a}$
	$\pi^2 \left[ D_{11} \frac{n^2}{a^2} + 5.139D_{22} \frac{a^2}{n^2 b^4} + 2.62(D_{11} + 2D_{66}) \right]$	$w(x, y) = \sum_{n=1}^{\infty} A_{mn} \left[ 1 - \cos \frac{2m\pi y}{b} \right] \sin \frac{n\pi x}{a}$
	$\frac{1.25 D_{22}}{n^2 a^4} + \frac{\pi^2 n^2 D_{11}}{a^2} + \frac{12 D_{66}}{b^2}$	$w(x, y) = \sum_{n=1}^{\infty} A_n y \sin \frac{n\pi x}{a}$

Table 2. Comparison between the analytical and the finite element results for effect of volume fractions, and different boundary conditions.

Boundary condition	CNTs volume fraction	$N_{cr}$ (KN) - ANL	$N_{cr}$ (KN) - FEM
s-s-s-s	$Cr=0.01$	59.546	54.1327
	$Cr=0.05$	218.38	201.95
	$Cr=0.1$	417	397.268
s-s-c-s	$Cr=0.01$	80.957	73.124
	$Cr=0.05$	288.17	273.36
	$Cr=0.1$	547.29	539.64
s-s-c-c	$Cr=0.01$	114.7	108.957
	$Cr=0.05$	393	379.16
	$Cr=0.1$	741.03	727.89
s-s-c-f	$Cr=0.01$	19.015	16.284
	$Cr=0.05$	65.59	61.14
	$Cr=0.1$	123.83	118.38

**7. Conclusion**

In this article, the critical buckling load of laminated composite plates reinforced by SWCNTs is investigated using both the analytical and the finite element methods. The results show that the critical buckling load obtained from FEM is in good agreement with those obtained by the analytical solution. As the shear strains are ignored in the analytical procedure, the buckling load obtained by this method is higher than that of the finite element solution.

The following conclusions can be drawn from the present study:

- (1) For all of the boundary conditions considered, the aspect ratio of  $a/b=2$  and the orientation angle of  $45^\circ$  yield the highest critical buckling load. The critical buckling load, the optimized orientation angle and the optimized mode shape decrease with decreasing the aspect ratio.
- (2) For constant aspect ratio and CNTs volume fraction, the highest critical buckling load occurs for the case in which two

parallel edges have clamped supported ( $s-s-c-c$ ).

(3) The lowest critical buckling load occurs for ( $s-s-s-f$ ) supported. For the ( $s-s-s$ ) supported case and aspect ratio of  $a/b=2$ , the optimized orientation angle for the best buckling load is  $45^\circ$  and the buckling occurs in the second mode. For the aspect ratio of  $2/3$ , however, the optimized orientation angle decreases to  $30^\circ$  and the buckling occurs in the first mode. For the aspect of  $1/2$ , the highest buckling load occurs when CNTs are arranged in the load direction. For all other boundary conditions, the optimized CNTs orientation angle changes by varying the aspect ratio. However, considering clamped edges instead of simply support ones, increases the critical buckling load of CNTRC plate.

(4) Non uniform dispersion of CNTs in the polymer matrix decreases the critical buckling load. Moreover, it increases the difference between the critical buckling loads obtained by the analytical method and the FEM. However, for low CNTs volume fractions, uniform dispersion does not have a significant effect on the critical buckling load; this is despite the fact that

Table 3. Effect of the CNTs angle on the buckling load for different mode shapes, aspect ratios, and boundary conditions assuming constant volume fractions.

Boundary condition	Aspect ratio	Mode shapes					Optimized buckling load	Optimized angle	Optimized mode shape
		CNTs orientation angle							
		n=1	n=2	n=3	n=4	n=5	$N_{Cro}$	$\theta_o$	$n_o$
s-s-s-s	a/b=2	0-33	34-53	54-64	64-77	78-90	834	45	2
	a/b=3/2	0-43	44-61	62-81	82-90	-	663.54	44	2
	a/b=1	0-56	57-90	-	-	-	417	45	1
	a/b=2/3	0-79	80-90	-	-	-	335.6	30	1
	a/b=1/2	0-90	-	-	-	-	410.9	0	1
s-s-c-s	a/b=2	0-25	26-44	45-55	56-64	65-90	1120.2	48	2
	a/b=3/2	0-35	36-53	54-65	66-90	-	800	42	2
	a/b=1	0-49	50-53	54-90	-	-	563.5	49	1
	a/b=2/3	0-62	63-90	-	-	-	373	36	1
	a/b=1/2	0-62	63-90	-	-	-	413.17	0	1
s-s-c-c	a/b=2	0-17	18-38	39-48	49-57	58-90	1304.4	45	3
	a/b=3/2	0-29	30-47	48-59	60-68	69-90	1000	47	3
	a/b=1	0-42	43-61	62-80	81-90	-	711.62	43	2
	a/b=2/3	0-56	57-90	-	-	-	420.41	56	1
	a/b=1/2	0-67	68-90	-	-	-	416.35	0	1
s-s-c-f	a/b=2	0-51	52-70	71-90	-	-	214.05	50	1
	a/b=3/2	0-60	61-90	-	-	-	156.58	35	1
	a/b=1	0-90	-	-	-	-	204.68	0	1
	a/b=2/3	0-90	-	-	-	-	304.32	0	1
	a/b=1/2	0-90	-	-	-	-	404.74	0	1

Table 4. Effect of the CNTs agglomeration in the polymer matrix reinforced by CNTs with volume fraction of  $C_r = 0.1$ .

	Inclusion volume to total volume ratio			CNTs volume fraction in the inclusion		
	$\xi = 1$	$\xi = 0.8$	$\xi = 0.4$	$\zeta = 1$	$\zeta = 0.7$	$\zeta = 0.4$
$\bar{E}(Gpa)$	8.3398	4.6051	1.9597	2.3806	7.6375	8.1496
V	0.2798	0.2868	0.3033	0.2986	0.28	0.2813
$N_{Cro}$ (KN) - ANL	160.74	89.143	38.308	46.433	147.18	157.22
$N_{Cro}$ (KN) - FEM	160.44	83.63	31.95	40.18	141.17	155.34

for the non uniform CNTs dispersion, the critical buckling load decreases exponentially with increasing the volume fraction.

**Acknowledgment**

The authors would like to thank the referees for their valuable comments, and also, the Iranian Nanotechnology Development Committee for their financial support.

**References**

[1] D. Qian, G. J. Wagner, W. K. Liu, M. F. Yu and R. S. Ruoff, Mechanics of Carbon Nanotubes, *Applied Mechanics Reviews*, 55 (2002) 495-533.

[2] R. Saito, G. Dresselhaus and M. S. Dresselhaus, *Physical Properties of Carbon Nanotubes*, Imperial College Press, London (1998).

[3] H. Wan, F. Delale and L. Shen, Effect of CNT length and CNT-matrix interphase in Carbon nanotube (CNT) reinforced composites, *Mechanics Research Communications*, 32 (2005) 481-489.

[4] H. Tan, Y. Huang, C. Liu and P. H. Geubelle, The Mori-Tanaka method for composite materials with nonlinear interface debonding, *International Journal of Plasticity*, 21 (2005) 1890-1918.

[5] H. Tan, L.Y. Jiang, Y. Huang, B. Liu and K.C. Hwang, The

effect of van der Waals-based interface cohesive law on carbon nanotube-reinforced composite materials, *Composites Science and Technology*, 67 (2007) 2941-2946.

- [6] W.B. Lu, J. Wua, J. Song, K. C. Hwang, L. Y. Jiang and Y. Huang, A cohesive law for interfaces between multi-wall carbon nanotubes and polymers due to the van der Waals interactions, *Computer Methods in Applied Mechanics and Engineering*, 197 (2008) 3261-3267.
- [7] A. Salehi-Khojin and N. Jalili, Buckling of boron nitride nanotube reinforced Piezoelectric polymeric composites subject to combined electro-thermo-mechanical loadings, *Composites Science and Technology*, 68 (2008) 1489-1501.
- [8] A. Haque and A. Ramasetty, Theoretical study of stress transfer in carbon nanotube reinforced polymer matrix composites, *Composite Structures*, 71 (2005) 68-77.
- [9] X. F. Li, K. T. Lau and Y. S. Yin, Mechanical properties of epoxy-based composites using coiled carbon nanotubes, *Composites Science and Technology*, 68 (2008) 2876-2881.
- [10] L. L. Ke, J. Yang and S. Kitipornchai, Nonlinear free vibration of functionally graded carbon nanotube-reinforced composite beams, *Composite Structures*, 92 (2010) 676-683.
- [11] A. H. Sofiyev, Torsional buckling of cross-ply laminated orthotropic composite cylindrical shells subject to dynamic loading, *European Journal of Mechanics A/Solids*, 22 (2003) 943-951.
- [12] T. Ozben, Analysis of critical buckling load of laminated composites plate with different boundary conditions using FEM and analytical methods, *Computational Materials Science*, 45 (2009) 1006-1015.
- [13] H. S. Shen and C. L. Zhang, Thermal buckling and post buckling behavior of functionally graded carbon nanotube-reinforced composite plates, *Materials & Design*, 31 (2010) 3403-3411.
- [14] T. Mori and K. Tanaka, Average Stress in Matrix and Average Elastic Energy of Materials With Misfitting Inclusions, *Acta Metallurgica*, 21 (1973) 571- 574.
- [15] L. P. Kollar and G. S. Springer, *Mechanics of Composite Structures*, Cambridge University Press, NY, USA, 2003.
- [16] D. L. Shi, X. Q. Feng, Y. Y. Huang, K. C. Hwang and H. Gao, The Effect of Nanotube Waviness and Agglomeration on the Elastic Property of Carbon Nanotube-Reinforced Composites, *Transactions of the ASME, Journal of Engineering Materials and Technology*, 126 (2004) 250-257.
- [17] J. R. Vinson, *The behavior of thin walled structures, beams, plates and shells*, Kluwer Academic pub.1989.
- [18] J. George, *An introduction to elastic Stability of Structures*, Prentice - Hall, 1976.
- [19] J. N. Reddy, *Theory and analysis of elastic plates and shells*, Second edition, CRC PRESS, USA , 2007.
- [20] J. N.Reddy, *An Introduction to The Finite Element Method*, McGraw-Hill Inc, 1993.
- [21] V. N. Popov, V. E. Doren and M. Balkanski, Elastic Properties of Crystals of Single-Walled Carbon Nanotubes, *Solid State Communications*, 114 (2000) 395-399.

## Appendix

### A.1 Derivation matrix

$$[d^0] = \begin{bmatrix} \frac{\partial}{\partial x} & 0 & \frac{1}{2}w_{0,x} \frac{\partial}{\partial x} & 0 & 0 \\ 0 & \frac{\partial}{\partial y} & \frac{1}{2}w_{0,y} \frac{\partial}{\partial y} & 0 & 0 \\ 0 & 0 & \frac{\partial}{\partial y} & 0 & 1 \\ 0 & 0 & \frac{\partial}{\partial x} & 1 & 0 \\ \frac{\partial}{\partial y} & \frac{\partial}{\partial x} & w_{0,y} \frac{\partial}{\partial x} & 0 & 0 \end{bmatrix}$$

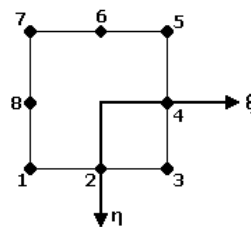
$$[d^1] = \begin{bmatrix} 0 & 0 & 0 & \frac{\partial}{\partial x} & 0 \\ 0 & 0 & 0 & 0 & \frac{\partial}{\partial y} \\ 0 & 0 & 0 & 0 & 0 \\ 0 & 0 & 0 & 0 & 0 \\ 0 & 0 & 0 & \frac{\partial}{\partial y} & \frac{\partial}{\partial x} \end{bmatrix}$$

$$[d^2] = -\frac{4}{h^2} \begin{bmatrix} 0 & 0 & 0 & 0 & 0 \\ 0 & 0 & 0 & 0 & 0 \\ 0 & 0 & \frac{\partial}{\partial y} & 0 & 1 \\ 0 & 0 & \frac{\partial}{\partial x} & 1 & 0 \\ 0 & 0 & 0 & 0 & 0 \end{bmatrix}$$

$$[d^3] = \begin{bmatrix} 0 & 0 & w_{0,x} \frac{\partial}{\partial x} & \frac{\partial}{\partial x} & 0 \\ 0 & 0 & w_{0,y} \frac{\partial}{\partial y} & 0 & \frac{\partial}{\partial y} \\ 0 & 0 & 0 & 0 & 0 \\ 0 & 0 & 0 & 0 & 0 \\ 0 & 0 & 2w_{0,y} \frac{\partial}{\partial x} & \frac{\partial}{\partial y} & \frac{\partial}{\partial x} \end{bmatrix}$$

(A1)

### A.2 Shape function for serendipity element



$$N_1 = \frac{1}{4}(1-\zeta)(1+\eta)(-\zeta+\eta-1)$$

$$N_2 = \frac{1}{2}(1-\zeta^2)(1+\eta)$$

$$N_3 = \frac{1}{4}(1+\zeta)(1+\eta)(\zeta+\eta-1)$$

$$\begin{aligned}
 N_4 &= \frac{1}{2}(1 + \xi)(1 - \eta^2) \\
 N_5 &= \frac{1}{4}(1 + \xi)(1 - \eta)(\xi - \eta - 1) \\
 N_6 &= \frac{1}{2}(1 - \xi^2)(1 - \eta) \\
 N_7 &= \frac{1}{4}(1 - \xi)(1 - \eta)(-\xi - \eta - 1) \\
 N_8 &= \frac{1}{2}(1 - \xi)(1 - \eta^2)
 \end{aligned} \tag{A2}$$

$$\{\varphi\} = [N] \{\Phi^{(e)}\} \tag{A3}$$

where

$$[N] = \begin{bmatrix} N_1 & 0 & 0 & 0 & 0 & \dots & N_8 & 0 & 0 & 0 & 0 \\ 0 & N_1 & 0 & 0 & 0 & \dots & 0 & N_8 & 0 & 0 & 0 \\ 0 & 0 & N_1 & 0 & 0 & \dots & 0 & 0 & N_8 & 0 & 0 \\ 0 & 0 & 0 & N_1 & 0 & \dots & 0 & 0 & 0 & N_8 & 0 \\ 0 & 0 & 0 & 0 & N_1 & \dots & 0 & 0 & 0 & 0 & N_8 \end{bmatrix} \tag{A4}$$

Displacement in the point of each element

$$\{\Phi^{(e)}\}^T = \langle u_0^{(1)} v_0^{(1)} w_0^{(1)} \psi_x^{(1)} \psi_y^{(1)} \dots u_0^{(8)} v_0^{(8)} w_0^{(8)} \psi_x^{(8)} \psi_y^{(8)} \rangle \tag{A5}$$

**A.3 B matrix**

$$[B^0] = \begin{bmatrix} N_{1,x} & 0 & \frac{1}{2}N_{1,x}w_{0,x} & 0 & 0 & \dots & N_{8,x} & 0 & \frac{1}{2}N_{8,x}w_{0,x} & 0 & 0 \\ 0 & N_{1,y} & \frac{1}{2}N_{1,y}w_{0,y} & 0 & 0 & \dots & 0 & N_{8,y} & \frac{1}{2}N_{8,y}w_{0,y} & 0 & 0 \\ 0 & 0 & N_{1,y} & 0 & N_1 & \dots & 0 & 0 & N_{8,y} & 0 & N_8 \\ 0 & 0 & N_{1,x} & N_1 & 0 & \dots & 0 & 0 & N_{8,x} & N_8 & 0 \\ N_{1,y} & N_{1,x} & N_{1,x}w_{0,y} & 0 & 0 & \dots & N_{8,y} & N_{8,x} & N_{8,x}w_{0,y} & 0 & 0 \end{bmatrix}$$

$$[B^1] = \begin{bmatrix} 0 & 0 & 0 & N_{1,x} & 0 & \dots & 0 & 0 & 0 & N_{8,x} & 0 \\ 0 & 0 & 0 & 0 & N_{1,y} & \dots & 0 & 0 & 0 & 0 & N_{8,y} \\ 0 & 0 & 0 & 0 & 0 & \dots & 0 & 0 & 0 & 0 & 0 \\ 0 & 0 & 0 & 0 & 0 & \dots & 0 & 0 & 0 & 0 & 0 \\ 0 & 0 & 0 & N_{1,y} & N_{1,x} & \dots & 0 & 0 & 0 & N_{8,y} & N_{8,x} \end{bmatrix}$$

$$[B^2] = -\frac{4}{h^2} \begin{bmatrix} 0 & 0 & 0 & 0 & 0 & \dots & 0 & 0 & 0 & 0 & 0 \\ 0 & 0 & 0 & 0 & 0 & \dots & 0 & 0 & 0 & 0 & 0 \\ 0 & 0 & N_{1,y} & 0 & N_1 & \dots & 0 & 0 & N_{8,y} & 0 & N_8 \\ 0 & 0 & N_{1,x} & N_1 & 0 & \dots & 0 & 0 & N_{8,x} & N_8 & 0 \\ 0 & 0 & 0 & 0 & 0 & \dots & 0 & 0 & 0 & 0 & 0 \end{bmatrix} \tag{A6}$$



**Ali Ghorbanpour Arani** received his BS degree from Sharif University of Technology in Tehran, Iran, in 1988. He then received his MS degree from Amirkabir University of Technology in Tehran, Iran, in 1991 and his Ph.D degree from the Esfahan University of Technology in Esfahan, Iran, in 2001.

Dr. Ali Ghorbanpour Arani is currently a Professor in Mechanical Engineering Department of University of Kashan in Kashan, Iran. His current research interests are stress analyses, stability and vibration of nanotubes, and FGMs.



**Sh. Maghamikia** received his BS degree from Islamic Azad University in Tehran, Iran, in 2007. He received his MS degree from University of Kashan in Kashan, Iran, in 2009. His research interests include nanomechanics, functionally graded materials (FGMs) and finite element method (FEM).



**Mehdi Mohammadimehr** received his BS degree from the University of Kashan in Kashan, Iran, in 2002. He then received his MS and Ph.D degrees from Shahid Bahonar University of Kerman in Kerman, Iran, in 2004 and 22 May 2010. Dr. Mehdi Mohammadimehr is currently an Assistant Professor in Mechanical Engineering Department of University of Kashan in Kashan, Iran. His research interests include elasticity, plasticity, continuum mechanics, nanomechanics, composite materials, functionally graded materials (FGMs), beams, plates and shells theories, buckling, post-buckling and vibration analyses of carbon nanotubes (CNTs), and finite element method (FEM).

Dr. Mehdi Mohammadimehr is currently an Assistant Professor in Mechanical Engineering Department of University of Kashan in Kashan, Iran. His research interests include elasticity, plasticity, continuum mechanics, nanomechanics, composite materials, functionally graded materials (FGMs), beams, plates and shells theories, buckling, post-buckling and vibration analyses of carbon nanotubes (CNTs), and finite element method (FEM).



**Ali Arefmanesh** received his BS degree from Sharif University of Technology in Tehran, Iran, in 1980. He then received his MS degree in 1987 and his Ph. D in 1992 from University of Delaware in Newark, DE, USA. Dr. Ali Arefmanesh is currently an Associate Professor in Mechanical Engineering Department of

University of Kashan in Kashan, Iran. His current research interests are computational mechanics, numerical simulations of fluid flow and heat transfer of nanofluid, and meshless numerical techniques.